

A simple integrated single-atom detector

Marco Wilzbach,^{1,2} Dennis Heine,^{1,2} Sönke Groth,² Xiyuan Liu,³ Björn Hessmo,^{1,2} and Jörg Schmiedmayer^{1,2}

¹Atominsttitut der Österreichischen Universitäten, Technische Universität Wien, Stadionallee 2, 1020 Wien, Austria

²Physikalisches Institut, Universität Heidelberg, Philosophenweg 12, 69120 Heidelberg, Germany

³Lehrstuhl für Optoelektronik, Universität Mannheim, 68131 Mannheim, Germany

We experimentally implement an integrated detector capable to detect single atoms with an efficiency of 56% and a signal-to-noise ratio of 275. We magnetically guide cold atoms through the focus of a tapered lensed fiber, mounted on the surface of an atom chip, where they are optically excited and emit bursts of fluorescent photons. Some of these photons are collected by another chip-mounted fiber and counted by a photon counter. Simple improvements will allow atom counting with close to unit efficiency.

PACS numbers: 03.75.-b, 42.50.Lc, 42.81.-i, 07.60.Vg

Counting single photons was one of the starting points of quantum optics [1]. The ability to efficiently detect single particles is of fundamental importance to many branches of science. In particular, it is one of the key ingredients for quantum technologies [2].

Detecting cold neutral atoms is usually achieved by illumination with near-resonant light, followed by a measurement of the absorption, phase shift or fluorescence. Absorption measurements have been realized in many different configurations, but single pass absorption does not allow to detect single atoms [3]. Placing an optical cavity around the detection region significantly enhances the absorption signal and single atom sensitivity can be achieved. [4, 5, 6, 7, 8, 9, 10, 11, 12]. The active alignment of the cavities is technically challenging.

Fluorescence detection of tightly trapped atoms or ions is very efficient, many photons can be collected when the atom remains localized. It is the method of choice for many single atom or ion experiments [13, 14, 15, 16, 17, 18, 19, 20, 21]. Cavities can be used to enhance the collection efficiency [10, 11]. A free neutral atom is significantly harder to detect because only a few photons can be scattered before the atom moves significantly and the few collected photons are difficult to distinguish from background light leading to a low signal-to-noise ratio.

In this letter we present an optical fiber based fluorescence detector integrated on an atom chip [22, 23] that achieves single atom detection with an efficiency of 56%, a high signal-to-noise ($S/N > 275$) and bandwidth of ~ 75 kHz.

In an ideal, background free, fluorescence detector a single detected photon implies that an atom is present in the detection region. In a physical implementation of a detector the background light has to be reduced to an absolute minimum while simultaneously keeping a high collection efficiency for the fluorescence to reach high signal-to-noise ratio.

In our setup we achieve a background suppression of better than 10^{-10} , essentially eliminating influence of stray light. This is realized by using a tapered lensed fiber to deliver excitation light only to a small detection region and a multi-mode fiber to efficiently collect the fluorescent photons from this small excitation volume. The background noise in our measurements is essentially determined by the dark count rate of the photon counter (APD). All other sources of background

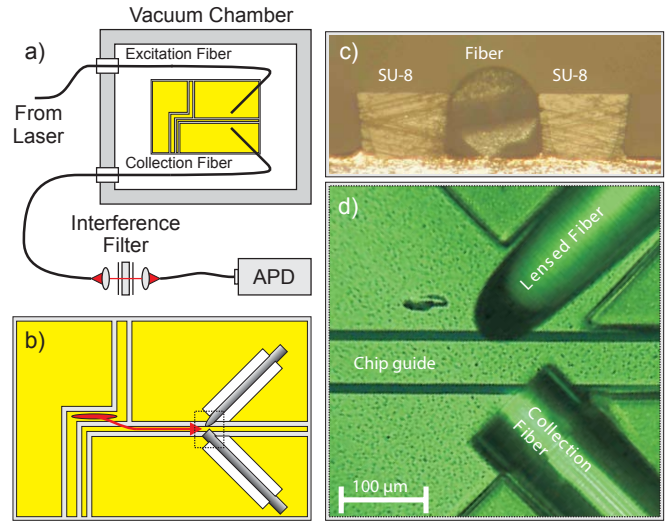


Figure 1: The integrated detector: a) Basic layout of the detector and the atom chip in the vacuum chamber. The excitation light is delivered to the tapered lensed fiber via a feed-through into the vacuum chamber [24]. The light scattered by the atoms is collected by a multi-mode fiber that guides the light out of the vacuum chamber. To eliminate background light and to protect the photon counter, an interference filter with a 3 nm wide transmission window (FWHM) centered at 780 nm is inserted before the photon counter (APD). b) A schematic layout of the atom chip. Atoms are initially trapped in a magnetic trap generated by a Z-shaped wire. A magnetic guide transports the atoms to the focus of the tapered lensed fiber mounted on the chip. The current in the guiding wire and external bias fields are adjusted to overlap the atomic guide with the focus. c) Image showing a cross-section illustrating the mounting of the optical fiber by the the undercut SU-8 structures. d) A microscopy image of the detection region on the chip.

noise are efficiently suppressed. This extremely low background allows high fidelity detection of a single atom by collecting just a single fluorescence photon out of the many photons scattered by an atom.

The detector is fully integrated on the atom chip by mounting the two fibers on the chip surface in lithographically defined holders fabricated from SU-8 resist. The undercut sidewall profile with a height of 90 μm (greater than the 62.5

μm radius of the fiber) clamps the fiber to the surface (See Fig. 1c, and 1d). The SU-8 structures allow a very accurate and stable passive alignment with accuracies better than a few ten nanometers and provide exceptional mechanical stability [25, 26]. The quality of the structures was assessed with a fiber cavity inserted in a holding structure. Temperature changes of up to 100 °C and sizable temperature gradients resulted in no measurable misalignment of the fibers. Long term stability (under experimental conditions) of over one year has been observed.

The tapered lensed fiber used to excite the atoms is a single-mode fiber with a rounded tip forming a high-quality lens with a focal length of 40 μm and a mode waist of 2.5 μm . The fluorescent photons are collected using a standard multimode fiber with a numerical aperture (NA) of 0.275. The optical collection efficiency of this fiber is 1.9%. Figure 1d shows a microscopy image of the detection region.

The multimode fiber sends the collected photons through an interference filter to the photon counter as illustrated in Fig. 1a. The overall photon detection efficiency of this setup is $p_{\text{det}} = 0.8\%$.

The detection region is situated 62.5 μm above a magnetic guide, 5.5 mm away from the magnetic chip trap used to trap and prepare the atoms.

In the experiment we follow our standard procedure [27], where ^{87}Rb atoms are first laser cooled in a magneto-optic trap, optically pumped into the $|F = 2, m_F = 2\rangle$ state and transferred to a Ioffe-Pritchard type magnetic trap generated by a Z-shaped wire on the chip surface. The atoms in the magnetic trap are released into a magnetic guide where the atomic cloud can expand towards the detector. The phase space density in the magnetic trap and guide is always less than 10^{-6} . See Fig. 1b for a schematic description of the chip. Over the next 1000 ms atoms pass the detector and the fluorescent photons are collected by the multi-mode fiber and counted.

The position of the magnetic guide above the chip surface is aligned with the focus of the tapered lensed fiber at the detection region by adjusting the current through the chip wire I_g and the strength of the external magnetic field perpendicular to the wire B_{\perp} . The guide is located at height $r_0 = \frac{\mu_0 I_g}{2\pi B_{\perp}}$, where μ_0 is the vacuum permeability [23]. In the focus of the lensed fiber the atoms are excited by a laser operating near the rubidium D2 transition from hyperfine state $F = 2$ to $F' = 3$. The experiment is repeated several times to measure the photon statistics. A typical signal is shown in Fig. 2.

One striking observation from measurements with this detector is that stray light effects on the guided atoms can be completely neglected. The magnetically guided atoms are not expelled from the guide by stray light. This stability is quite remarkable, because magnetic traps are extremely sensitive to the presence of light close to resonance with an atomic transition. On average, scattering of a little more than a single photon is sufficient to pump the atom into a magnetically untrapped state, removing it from the magnetic guide.

When an atom arrives at the detector, it absorbs and then re-emits photons. A few of these photons are counted by the

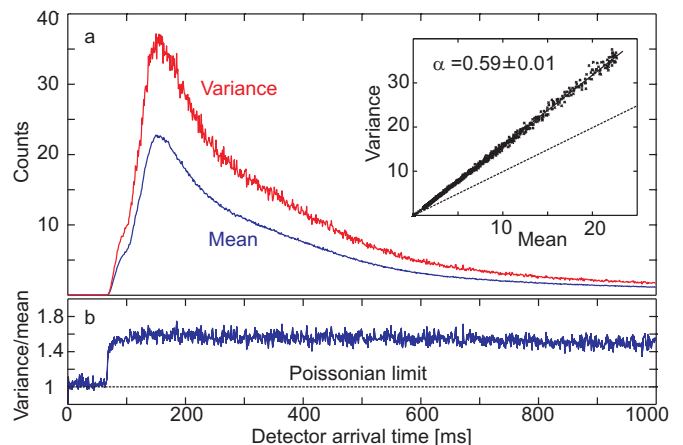


Figure 2: Mean and variance for the photons. a) By repeating the measurement 200 times, the mean and variance of the collected photons are obtained. Here, a time bin of 100 μs has been used. The lower (blue) curve shows the mean photon count for these 200 experimental runs and the upper (red) curve shows the variance for the same runs. The inset shows a plot of the variance as a function of the mean values. A linear fit of the data gives the parameter α . In this case the slope of the curve is equal to 1.59 ± 0.01 with a confidence interval of 99%. From equation (1), the value $\alpha = 0.59$ is deduced. The dashed line corresponds to Poissonian statistics. b), If the detector efficiency is independent of atomic density, then the variance divided by the mean should stay constant when the atomic density is varied. This plot shows that $1 + \alpha$ remains approximately constant (at 1.59) even when the atom density varies by one order of magnitude. The small deviation from the constant value is due to APD dark counts. Before the atoms arrive at the detector, one can see that the detector noise obeys Poissonian statistics.

APD. After a certain time τ the atom will leave the detection region. Except for random background counts with very low probability the detector sees no further light until the next atom arrives. Therefore for small atom flux the photon count distribution should reflect both: The time structure of the collected photons from a single atom at time scales $\sim \tau$, and the distribution of the atoms at the long time scale ($\gg \tau$).

To analyze these features, it is useful to measure the noise and time correlations of the photon counts. In the experiments presented here we use thermal atoms in a multi-mode guide with (typically $> 10^3$ transverse modes are occupied). Consequently, the atoms exhibit Poissonian statistics, and the photon statistics gives reliable information about the detection process.

One would expect the photon noise to be super-Poissonian because more than one photon can be scattered from a single atom. Starting from Mandel's formula [28] we can relate the variance and mean of the photon counts directly to the average number of photons detected from each atom.

The photon flux during time intervals much times longer than the atomic life time is described by a Poissonian probability distribution $P_{PD}(\langle n \rangle, n) = \frac{\langle n \rangle^n}{n!} \exp[-\langle n \rangle]$. The mean photon number and the variance are both equal to $\langle n \rangle$.

This is only valid if $\langle n \rangle$ is constant in time [29]. It does

not hold when the fluorescent photons come from a random flow of atoms described by a statistical distribution $P_{\text{atom}}(m)$. To describe the photon statistics of these photons, Mandel's formula must be used [28]: $P(n) = \sum_m P(n|m)P_{\text{atom}}(m)$ where $P(n|m)$ is the conditional probability of emitting n photons when the observation region contains m atoms. To describe this situation a parameter α is introduced describing the average number of photons detected from each atom, i.e. defined by the relation $\langle n \rangle = \alpha m$. This leads to the photon distribution

$$P(n|m) = \frac{(\alpha m)^n}{n!} e^{-\alpha m}.$$

Calculating the mean and the variance using Mandel's formula one obtains the ratio

$$\frac{\text{var}(N_{\text{photons}})}{\langle N_{\text{photons}} \rangle} = 1 + \alpha \frac{\text{var}(N_{\text{atoms}})}{\langle N_{\text{atoms}} \rangle}$$

for the photon distribution. When the atoms obey Poissonian statistic, as in our experiments, the photon statistics gives directly the mean number of photons detected from each atom α by

$$\frac{\text{var}(N_{\text{photons}})}{\langle N_{\text{photons}} \rangle} = 1 + \alpha. \quad (1)$$

From α it is possible to determine the atom detection efficiency. If there is one atom in the detection region, it will generate at least one photon count with a probability $P_{\text{detection}} = 1 - \exp(-\alpha)$.

From the photon statistics in the data shown in Fig. 2, one obtains $\alpha=0.59$ for an excitation laser with 14 MHz red-tuning and an intensity of 1.4 nW. For on resonant excitation one finds $\alpha=0.81$ and $P_{\text{detection}} = 0.56$.

The total number of photons scattered by the atoms before leaving the detection region can be obtained by measuring the ratio of the fluorescence counts for $F=2 \rightarrow F'=1$ and the $F=2 \rightarrow F'=3$ transitions. On the $F=2 \rightarrow F'=1$ transition an atom scatters slightly more than one photon before being optically pumped into the other hyperfine ground state. This ratio indicates that each atom scatters ~ 70 photons (~ 97 photons) at 14 MHz detuning (resonance) before it leaves the detector. These numbers are in good agreement with the above given photon detection efficiency, $p_{\text{det}} = 0.8\%$. In addition, the value of α was confirmed by independent global atom number measurements using absorption imaging.

The fluorescence decay, as an atom leaves the detection region, can be investigated by analyzing the arrival-time distribution of the photons. In the case of an uncorrelated process, the probability of finding a time interval of n bins that contain no photons is given by $P_{\text{TI}}(n) = (1 - p_0)p_0^n$, where p_0 is the probability for an empty bin. This means that $\log P_{\text{TI}}(n)$ is a linear function of n . In Fig. 3 we see that short time intervals are over-represented in comparison to any uncorrelated process. This confirms the above simple model.

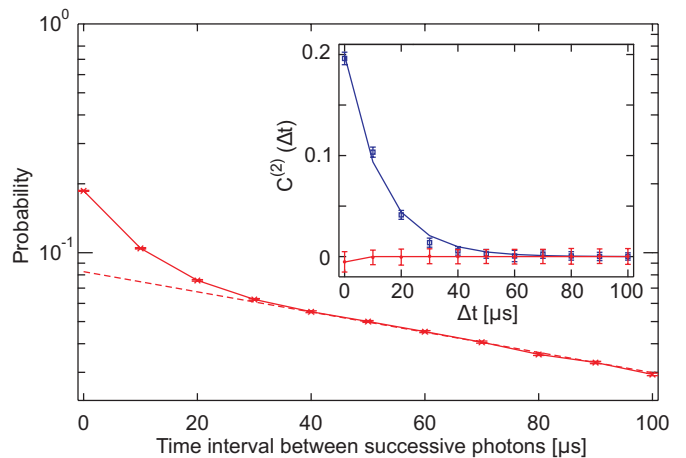


Figure 3: The data points in the main figure show the probabilities for finding different time intervals between successive photon detections. The points are connected by a line to guide the eye. The dashed line is a fit obtained by assuming an uncorrelated photon distribution. Error bars represent statistical standard deviations. Short time intervals are more likely for the photon flux generated by the atoms than for an uncorrelated photon flux with the same mean intensity. The inset shows the correlation function defined by equation (2) for the data generating the time interval histogram. The time constant of the correlation is 13 μs . This corresponds to a detection bandwidth of 75kHz. The lower curve in the inset is the correlation of laser light directly illuminating the photon counter.

The short-time behavior can also be analyzed by investigating the temporal correlations of the detected photons. The correlation function

$$C^{(2)}(t_n, t_m) = \frac{\langle (N_{\text{photons}}(t_n) - \mu_n)(N_{\text{photons}}(t_m) - \mu_m) \rangle}{\sqrt{\mu_n \mu_m}} - \delta_{nm}, \quad (2)$$

with $\mu_k = \langle N_{\text{photons}}(t_k) \rangle$, is zero for an uncorrelated Poissonian process. The inset of Fig. 3 shows $C^{(2)}(\Delta t)$ for the last 100 ms of the data in Fig. 2 and supports that photon emission is bunched in short time intervals. The correlation decays as an exponential with a time constant of $\tau = 13 \mu\text{s}$. This time constant is equal to the mean time each atom interacts with the excitation laser, and gives the detection bandwidth $1/\tau = 75 \text{ kHz}$, which compares favorably to other atom detectors [15, 16, 30] where the bandwidth is around 1 kHz.

The lower curve of the inset is obtained by counting photons from the excitation laser. The Poissonian distribution of these counts demonstrates that the detector is fast enough to faithfully record the photon statistics and that the excitation intensity is constant in time.

The fiber based detector presented here has exceptionally low background noise. The dominating contribution in the present experiment is the dark counts of the specific photon counter used (Perkin-Elmer, SPCM-AQR-12), which gives a background of approximately 250 counts per second. This can be reduced to approximately 25 counts per second by using a

different, commercially available photon counter with lower noise.

When the excitation light is present, an additional one photon per nW of excitation light is collected per second which corresponds to a stray-light suppression of 10^{-10} . Consequently, using excitation intensities of 1-10 times the saturation intensity (reached at 325 pW in the fiber) contributes negligible background.

In addition black-body radiation from the rubidium dispensers contributes to the background with 40 counts per second. Switching off the dispensers during the detection eliminates this background. All other background sources are efficiently suppressed by the interference filter to nonmeasurable values. Therefore, the total background noise of the present detector is 290 counts per seconds. Defining the signal-to-noise as the instantaneous count rate from an individual atom divided by the background the experiment presented here archives a S/N of ~ 275 , which can easily be improved by at least an order of magnitude by using the better photon counter and switching off the dispensers.

This first implementation of a fully integrated on-chip atom detector can be significantly improved. The detection efficiency is mainly determined by the numerical aperture of the multimode collection fiber. Substituting the NA=0.275 fiber with a commercially available fiber with NA=0.6 the photon detection efficiency can be increased to 4.2% leading to $\alpha = 4$ counts per atom. Using two collection fibers with NA=0.6 increases these values to 8.4% and $\alpha = 8$. Such a configuration would give a single atom detection probability of $> 99.9\%$ and a signal-to-noise ratio of $> 10^4$. With these improvements, high fidelity atom counting and even distinguishing one atom from two atoms becomes feasible.

To conclude, we have built and evaluated an atom detector that is capable to efficiently detect a single atom by collecting just a single fluorescence photon. Low noise and high efficiency is achieved using fiber optics to create very selective excitation of the atoms and a small, matched observation volume. The detector efficiency of 56% and the bandwidth of 75 kHz have been determined by measuring the photon statistics of the atomic fluorescence. The atom counter is fully integrated in an atom chip experiment and mechanically very robust. Achieving a detection efficiency close to unity is straightforward by exchanging the collection fiber. The high efficiency, signal-to-noise ratio and bandwidth make the detector well suited for studies of correlated atomic systems and scalable quantum experiments on a single-atom or molecule level. Our detector can be seen as the matter wave optics equivalent to the APD in quantum optics.

We thank T. Fernholz, A Haase, and M. Schwarz for help in the early stages of the experiment and I. Bar-Joseph and K.H. Brenner for support in the fabrication of the chip and holding structures. We gratefully acknowledge financial support from Landesstiftung Baden-Württemberg, the and European Union (SCALA, Atomchip), and the FWF (PLATON).

-
- [1] L. Mandel and E. Wolf, *Optical Coherence and Quantum Optics* (Cambridge University Press, 1995).
 - [2] D. Bouwmeester, A. Ekert, and A. Zeilinger, *The Physics of Quantum Information: Quantum Cryptography, Quantum Teleportation, Quantum Computation* (Springer Verlag, Heidelberg, 2001).
 - [3] S. J. van Enk and H. J. Kimble, *Phys. Rev. A* **63**, 023809 (2001).
 - [4] H. Mabuchi, Q. Turchette, M. Chapman, and H. Kimble, *Opt. Lett.* **21**, 1393 (1996).
 - [5] P. Münstermann, T. Fischer, P. Maunz, P. Pinkse, and G. Rempe, *Phys. Rev. Lett.* **82**, 3791 (1999).
 - [6] C. Hood, T. Lynn, A. Doherty, A. Parkins, and H. Kimble, *Science* **287**, 1447 (2000).
 - [7] A. Öttl, S. Ritter, M. Köhl, and T. Esslinger, *Phys. Rev. Lett.* **95**, 90404 (2005).
 - [8] A. Haase, B. Hessmo, and J. Schmiedmayer, *Opt. Lett.* **31**, 268 (2006).
 - [9] T. Aoki, B. Dayan, E. Wilcut, W. Bowen, A. Parkins, T. Kippenberg, K. Valhala, and H. Kimble, *Nature(London)* **443**, 671 (2006).
 - [10] I. Teper, Y. Lin, and V. Vuletić, *Phys. Rev. Lett.* **97**, 23002 (2006).
 - [11] M. Trupke, J. Goldwin, B. Darquié, G. Dutier, S. Eriksson, J. Ashmore, and E. A. Hinds, *Phys. Rev. Lett.* **99**, 063601 (2007).
 - [12] Y. Colombe, T. Steinmetz, G. Dubois, F. Linke, D. Hunger, and J. Reichel, *Nature(London)* **450**, 272 (2007).
 - [13] W. Neuhauser, M. Hohenstatt, P. Toschek, and H. Dehmelt, *Phys. Rev. A* **22**, 1137 (1980).
 - [14] N. Schlosser, G. Reymond, I. Protsenko, and P. Grangier, *Nature* **411**, 1024 (2001).
 - [15] S. Kuhr, W. Alt, D. Schrader, M. Muller, V. Gomer, and D. Meschede, *Science* **293**, 278 (2001).
 - [16] M. Rowe, D. Kielpinski, V. Meyer, C. Sackett, W. Itano, C. Monroe, and D. Wineland, *Nature* **409**, 791 (2001).
 - [17] N. Schlosser, G. Reymond, and P. Grangier, *Phys. Rev. Lett.* **89**, 023005 (2002).
 - [18] D. Leibfried, R. Blatt, C. Monroe, and D. Wineland, *Rev. Mod. Phys.* **75**, 281 (2003).
 - [19] J. Volz, M. Weber, D. Schlenk, W. Rosenfeld, J. Vrana, K. Saucke, C. Kurtsiefer, and H. Weinfurter, *Phys. Rev. Lett.* **96**, 30404 (2006).
 - [20] M. Weber, J. Volz, K. Saucke, C. Kurtsiefer, and H. Weinfurter, *Phys. Rev. A* **73**, 43406 (2006).
 - [21] Y. R. P. Sortais et al., *Phys. Rev. A* **75**, 13406 (2007).
 - [22] R. Folman, P. Krüger, D. Cassettari, B. Hessmo, T. Maier, and J. Schmiedmayer, *Phys. Rev. Lett.* **84**, 4749 (2000).
 - [23] R. Folman, P. Krüger, J. Schmiedmayer, J. Denschlag, and C. Henkel, *Adv. At. Mol. Phys.* **48**, 263 (2002).
 - [24] E. Abraham and E. Cornell, *Appl. Opt.* **37**, 1762 (1998).
 - [25] X. Liu et al., *Appl. Opt.* **44**, 6857 (2005).
 - [26] M. Wilzbach et al., *Fortschritte der Physik* **54**, 746 (2006).
 - [27] S. Wildermuth et al., *Phys. Rev. A* **69**, 30901 (2004).
 - [28] L. Mandel and E. Wolf, *Rev. Mod. Phys.* **37**, 231 (1965).
 - [29] S. Kitson, P. Jonsson, J. Rarity, and P. Tapster, *Phys. Rev. A* **58**, 620 (1998).
 - [30] T. Bondo, M. Hennrich, T. Legero, G. Rempe, and A. Kuhn, *Opt. Comm.* **264**, 264 (2006).